CORROSION SCIENCE AND TECHNOLOGY, Vol.16, No.1(2017), pp.15~22
[Research Paper]
pISSN: 1598-6462 / eISSN: 2288-6524
DOI: https://doi.org/10.14773/cst.2017.16.1.15

Effects of Oxygen Partial Pressure on Oxidation Behavior of CMnSi TRIP Steel in an Oxidation-Reduction Scheme

Seong-Hwan Kim[1,††], Joo-Youl Huh[1,†], Myung-Soo Kim[2], and Jong-Sang Kim[2]

[1]*Department of Materials Science and Engineering, Korea University, Seoul 136-713, Republic of Korea*
[2]*POSCO Technical Research Laboratories, Gwangyang, Junnam 545-090, Republic of Korea*

(Received December 21, 2016; Revised January 24, 2017; Accepted January 27, 2017)

An oxidation-reduction scheme is an alternative approach for improving the galvanizability of advanced high-strength steel in the continuous hot-dip galvanizing process. Here, we investigated the effect of oxygen partial pressure (P_{O_2}) on the oxidation behavior of a transformation-induced plasticity steel containing 1.5 wt% Si and 1.6 wt% Mn during heating to and holding for 60 s at 700 °C under atmospheres with various P_{O_2} values. Irrespective of P_{O_2}, a thin amorphous Si-rich layer of Si-Mn-O was formed underneath the Fe oxide scale (a Fe_2O_3/Fe_3O_4 bilayer) in the heating stage. In contrast to Si, Mn tended to segregate at the scale surface as $(Fe,Mn)_2O_3$. The multilayered structure of $(Fe,Mn)_2O_3/Fe_2O_3/Fe_3O_4$/amorphous Si-Mn-O remained even after extended oxidizing at 700 °C for 60 s. Fe_2O_3 was the dominantly growing oxide phase in the scale. The enhanced growth rate of Fe_2O_3 with increasing P_{O_2} resulted in the formation of more Kirkendall voids in the amorphous Si-rich layer and a less Mn segregation at the scale surface. The mechanisms underlying the absence of FeO and the formation of Kirkendall voids are discussed.

Keywords: *oxidation, transformation-induced plasticity steel, oxidation-reduction scheme, oxygen partial pressure, amorphous Si oxide*

1. Introduction

The increasing demands for reducing fuel consumption and improving passenger safety have prompted automotive industries to develop advanced high-strength steels (AHSSs) for use in the structural parts of body-in-white (BIW). Among the currently developed AHSSs that contain various amounts of alloying elements, Mn, Si, and/or Al, transformation-induced plasticity (TRIP) steels possess combined properties of high strength and excellent formability, which are desirable for automotive applications [1]. The formable high-strength property of TRIP steels allows thinner-gauged sheets to be used in the BIW while maintaining the strength levels. However, to be used in automotive applications, the TRIP steels need corrosion protection, which is most effectively performed by means of a continuous hot-dip galvanizing process.

In the continuous hot-dip galvanizing process, prior to hot dipping, cold-rolled TRIP steel sheets undergo an intercritical annealing in the ferrite-austenite two-phase temperature range to achieve a multi-phase microstructure with a fraction of retained austenite after the galvanizing process. Although intercritical annealing is typically performed under a reducing gas mixture of N_2 and 5 – 10% H_2 to protect the steel sheet surface from being oxidized, alloying elements with a high affinity for oxygen, such as Mn, Si and Al, are still enriched and selectively oxidized at the steel sheet surface, leading to poor galvanizability of the steel sheets during the subsequent hot-dip process [2-5].

Therefore, extensive work has been performed to suppress the external oxidation of the alloying elements in AHSSs during intercritical annealing by controlling the dew point (DP) and composition of the annealing gases [6-13]. Increasing the DP in the annealing furnace could promote the alloying elements to shift from undergoing external oxidation to internal oxidation, and thus improve the galvanizability of AHSS sheets. However, external oxidation of the alloying elements could not be completely suppressed because of their high oxygen affinities. Alternatively, the oxidation-reduction scheme is a method of creating a pure Fe layer on the AHSS sheets after the intercritical anneal-

†Corresponding author: jyhuh@korea.ac.kr
††Present address: Hyundai Steel Co., Advanced Research Team, Dangjin 343-823, Republic of Korea

ing step so that the hot-dip galvanizability can be significantly improved [14]. In the oxidation-reduction process, a submicron-thick iron oxide layer is first formed on the steel sheet surface in the pre-heating stage using an oxidizing atmosphere, and then the iron oxide layer is reduced in the subsequent intercritical annealing. However, the pre-oxidation procedure in an oxidizing atmosphere can also cause the alloying elements to be enriched and oxidized at the iron oxide/steel interface. In contrast to the iron oxide, the oxides of the alloying elements cannot be reduced during intercritical annealing, and thus remain even after hot-dip galvanizing. The presence of an oxide layer (especially SiO_x) underneath the Zn coating overlay could result in easy detachment of the coating layer from the steel substrate during the stamping process. Therefore, for the oxidation-reduction scheme to be successfully used for AHSS sheets, it is important to control the internal oxidation behavior of the alloying elements in the pre-oxidation stage.

Although many studies have been reported on the oxidations of Fe [15], Fe-Si [16-18], and Fe-Mn [15,19] binary alloys, the short-term oxidation behaviors of AHSSs containing Mn and Si are still poorly understood. This study is aimed at examining the effect of the oxygen partial pressure (P_{O_2}) in the ambient gas on the oxidation behavior of a TRIP steel containing 1.6 wt% Mn and 1.5 wt% Si. For this purpose, oxidation of the TRIP steel was performed at 700 °C for 60 s under three different ambient gases: N_2 + 1% O_2, N_2 + 21% O_2 and 100% O_2.

Table 1 Chemical composition of the TRIP steel

Element	Fe	Mn	Si	C
wt%	Bal.	1.6	1.5	0.08

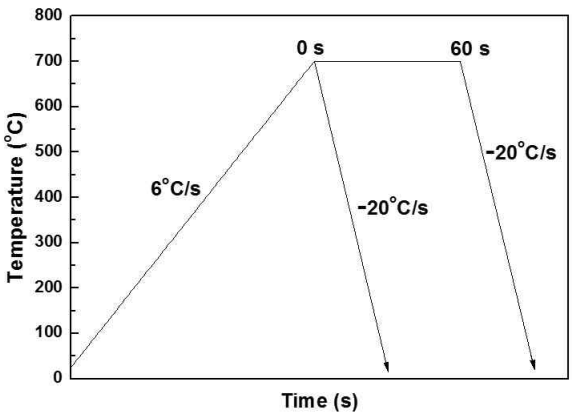

Fig. 1 Schematic representation of the temperature profile used for the oxidation in the present study. Samples were cooled down either upon ramping up to 700 °C or after isothermal holding at 700 °C for 60 s.

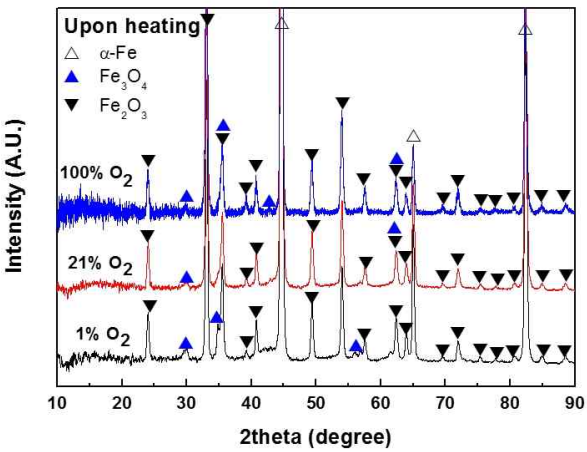

Fig. 2 GIXRD patterns for the samples cooled down immediately after heating to 700 °C under three different P_{O_2} conditions.

2. Experimental procedure

The 590-MPa-grade TRIP steel used in this study was provided in the form of cold-rolled full-hard sheets with dimensions of 120 mm × 200 mm × 1.5 mm by POSCO. The detailed composition of the TRIP steel is listed in Table 1. The steel sheets were cut into samples with dimensions of 50 mm × 50 mm, degreased with kerosene, and then ultrasonically cleaned in acetone. Oxidation of the samples was performed in a rapid thermal annealing (RTA) furnace under the steady flow (0.5 L/min) of 1 atm gas mixtures comprising N_2 and O_2 at various volume fractions of O_2: 1%, 21%, and 100%. Prior to heating, the RTA chamber was initially vacuum evacuated and purged thrice with the oxidation gas. Then, as shown schematically in Fig. 1, the samples were heated to 700 °C at a rate of 6 °C/s. Either upon reaching 700 °C or after holding at 700 °C for 60 s, the samples were cooled down to room temperature by flowing N_2 into the chamber to examine the oxidation behaviors during heating to 700 °C and isothermally holding at 700 °C.

The samples oxidized under the three different P_{O_2} (0.01, 0.21, and 1 atm) were analyzed using grazing incidence X-ray diffraction (GIXRD), glow discharge optical emission spectroscopy (GDOES), and transmission electron microscopy (TEM) along with an energy-dispersive X-ray spectroscopy (EDX). The cross-sectional TEM samples were prepared by a focused ion beam (FIB) milling after deposition of a Pt layer on the sample surface. The GIXRD analyses were performed using Cu-K_α radiation with a grazing incidence angle of 2°.

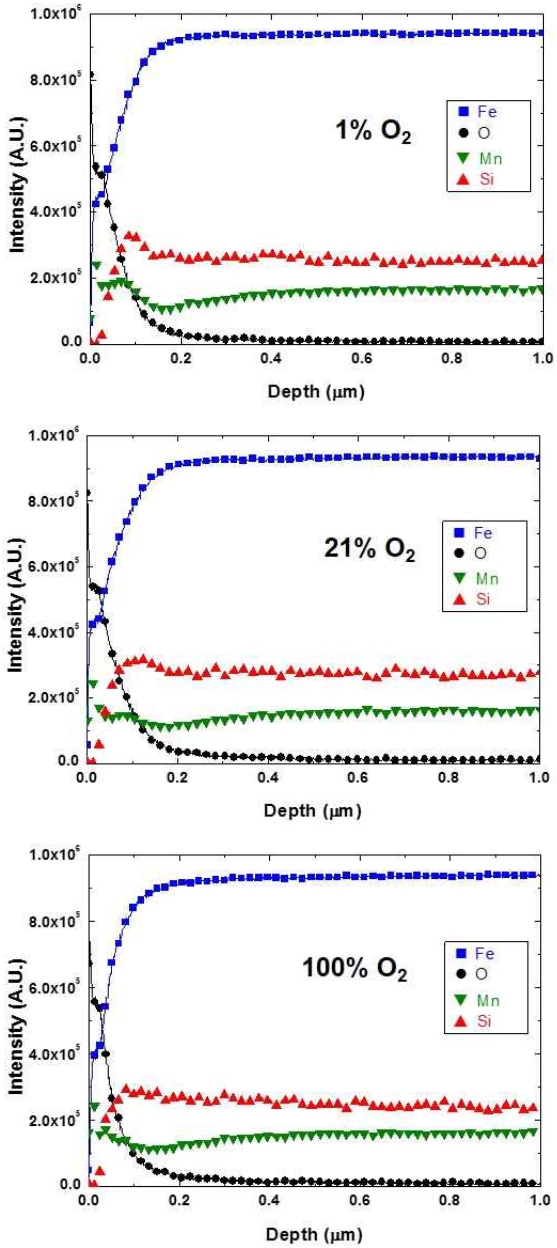

Fig. 3 GDOES depth profiles for elemental distributions in the scales formed in the heating stage under different ambient conditions: (a) N_2 + 1% O_2, (b) N_2 + 21% O_2, and (c) 100% O_2.

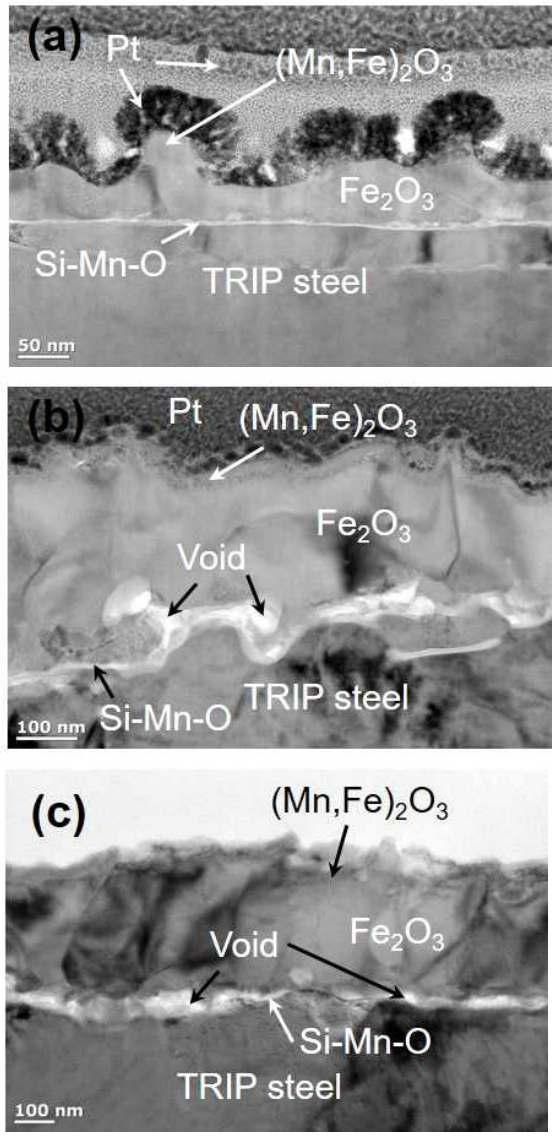

Fig. 4 Cross-sectional TEM micrographs showing the scales formed in the heating stage under different ambient conditions: (a) N_2 + 1% O_2, (b) N_2 + 21% O_2, and (c) 100% O_2. Note that the micrographs were taken at different magnifications.

3. Experimental results

3.1. Oxidation behavior in the heating stage

To examine the effect of the ambient oxygen content on the oxidation behavior in the heating stage, the TRIP steel samples were cooled down immediately after heating up to 700 °C at a rate of 6 °C/s under different P_{O_2}. As shown in Fig. 2, the samples heated under the different atmospheres exhibited similar GIXRD patterns where only oxide peaks of Fe_2O_3 and Fe_3O_4 were detected along with those of α-Fe. Strong intensities of the Fe_2O_3 peaks indicated that Fe_2O_3 was the major oxide phase in the scales formed under all atmospheres. No other oxides of the alloying elements Si and Mn were detected.

Fig. 3 compares the GDOES depth profiles of elemental distributions in the scales formed under the different atmospheres. By measuring the depth at which the Fe and O profiles cross each other, the scale thickness was estimated to be approximately 30 nm in all the samples. Mn exhibited a tendency to segregate at the top of the scale whereas Si segregated internally, underneath the scale. A

noticeable difference depending on the oxidizing atmospheres was the intensity and width of the Si peak underneath the scale; it became lower in intensity and broader in width with increasing P_{O_2}.

Fig. 4 shows the cross-sectional TEM micrographs of the scales depending on the oxidizing atmosphere. It is noted that the micrographs shown in Fig. 4 were taken at different magnifications. As expected from the GDOES results, all the samples exhibited a Si-rich layer with a bright contrast at the scale/steel interface. High-resolution images (not shown here) of the Si-rich layer revealed that the layer was amorphous. Considering the GDOES depth profiles of Mn shown in Fig. 3 that exhibited secondary intensity peaks at the same locations as those of the Si peaks, the Si-rich layer underneath the Fe-oxide scale should be an amorphous oxide layer of Si-Mn-O. It is interesting to note from Fig. 4 that micro-voids were present in the amorphous Si-Mn-O layer, their number increasing with increasing P_{O_2}. This increased void formation in the Si-Mn-O layer with increasing P_{O_2} is likely to be the reason for the GDOES depth profiles showing a lower and broad Si peak with increasing P_{O_2}. The mechanism behind the void formation will be further discussed in the following section.

In contrast to the scale thickness estimated from the GDOES depth profiles, the cross-sectional TEM micrographs shown in Fig. 4 revealed that the scale thickness was increased with increasing P_{O_2}. The scale thicknesses were determined from the cross-sectional TEM micrographs by dividing the area of the Fe-oxide scale by the linear interface length. As summarized in Table 2, the scale thickness increased from 58 nm to 374 nm by increasing P_{O_2} from 0.01 atm to 1 atm. The underestimation of the scale thicknesses from the GDOES profiles was likely attributed to an improper calibration of the depth profiling rate and the use of a large sputtering area (5 mm in diameter) covering local variations in the scale topology.

3.2. Oxidation behavior during isothermal oxidation at 700 °C

Table 2 Scale thicknesses measured from cross-sectional TEM micrographs

O_2 content (vol.%)	Scale thickness (nm)	
	Upon heating	After 60 s at 700 °C
1	58	144
21	147	510
100	374	1144

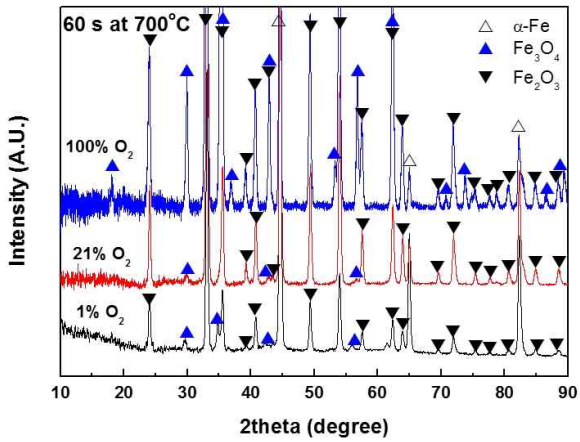

Fig. 5 GIXRD patterns for the samples after extended oxidation at 700 °C for 60 s under three different P_{O_2} conditions.

The TRIP steel samples heated to 700 °C at a rate of 6 °C/s were further oxidized isothermally at 700 °C for 60 s before being rapidly cooled down to room temperature. Fig. 5 shows the GIXRD patterns of the samples oxidized under the atmospheres with different P_{O_2}. The oxide peaks detected were Fe_2O_3 and Fe_3O_4 regardless of P_{O_2}. Compared to the corresponding GIXRD patterns in Fig. 2, the changes in the peak intensities of Fe_2O_3 and Fe_3O_4 after oxidizing further at 700 °C for 60 s were significantly dependent on the ambient P_{O_2}: no significant changes were observed for the 1% O_2 atmosphere, there was a significant increase of the Fe_2O_3 peaks in the case of the 21% O_2 atmosphere, and a significant increase in both the Fe_2O_3 and Fe_3O_4 peaks in the case of the 100% O_2 atmosphere. Surprisingly, there were no FeO peaks detected in this study. It is known that FeO is the predominant oxide phase formed when pure Fe is oxidized at temperatures above 570 °C [15]. The absence of FeO in this study was likely because of the presence of an amorphous Si-Mn-O layer at the scale/steel interface and will be further discussed later.

Fig. 6 shows the GDOES depth profiles obtained after the extended oxidation at 700 °C for 60 s. Noticeable differences from the profiles shown in Fig. 3 were the scale thickness and the distributions of Si and Mn. In contrast to the case of the 1% O_2 atmosphere (Fig. 6a), the 21% and 100% O_2 atmospheres (Fig. 6b and c, respectively) showed a significant growth of the Fe oxide scale after the extended oxidation, as determined from the depth at which the Fe and O profiles cross each other, which was in accordance with the GIXRD results. Regardless of the O_2 content in the oxidizing atmosphere, the alloying element Mn had a strong tendency to segregate at the scale surface during the extended oxidation at 700 °C, whereas

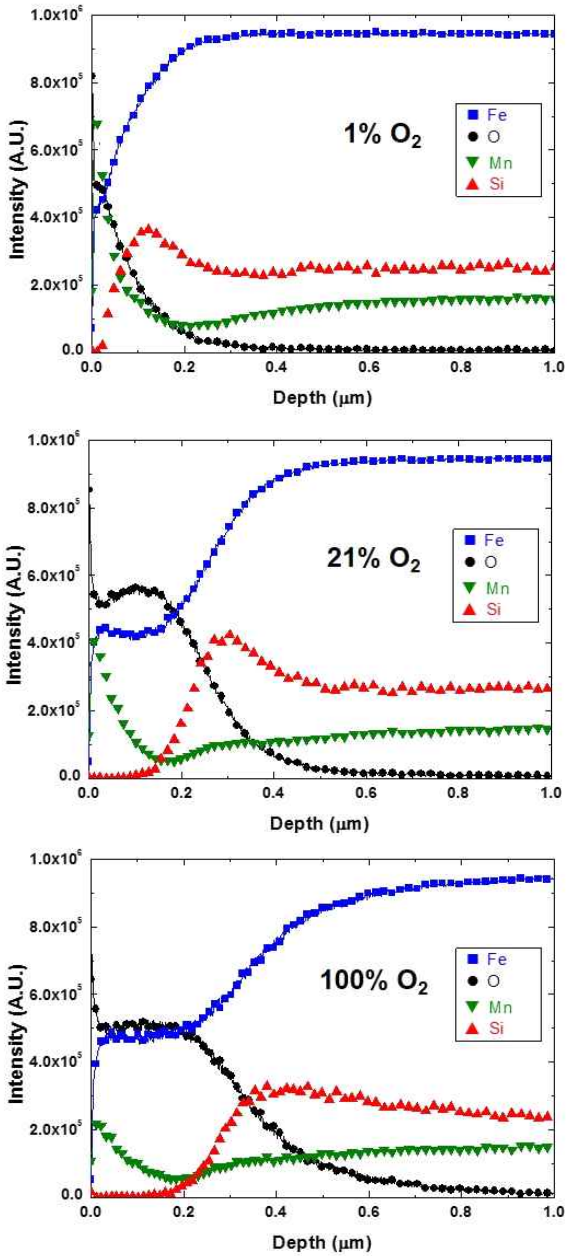

Fig. 6 GDOES depth profiles for elemental distributions in the scales formed after extended oxidation at 700 °C for 60 s under different ambient conditions: (a) N_2 + 1% O_2, (b) N_2 + 21% O_2, and (c) 100% O_2.

the alloying element Si was oxidized internally, underneath the Fe oxide scale. A comparison of the Mn intensities at the scale surface suggested that the surface segregation of Mn should become more significant by lowering P_{O_2} in the ambience, which was partly because of the reduced growth rate of the Fe oxide scale.

The microstructure of the scales formed after the extended oxidation was examined using cross-sectional

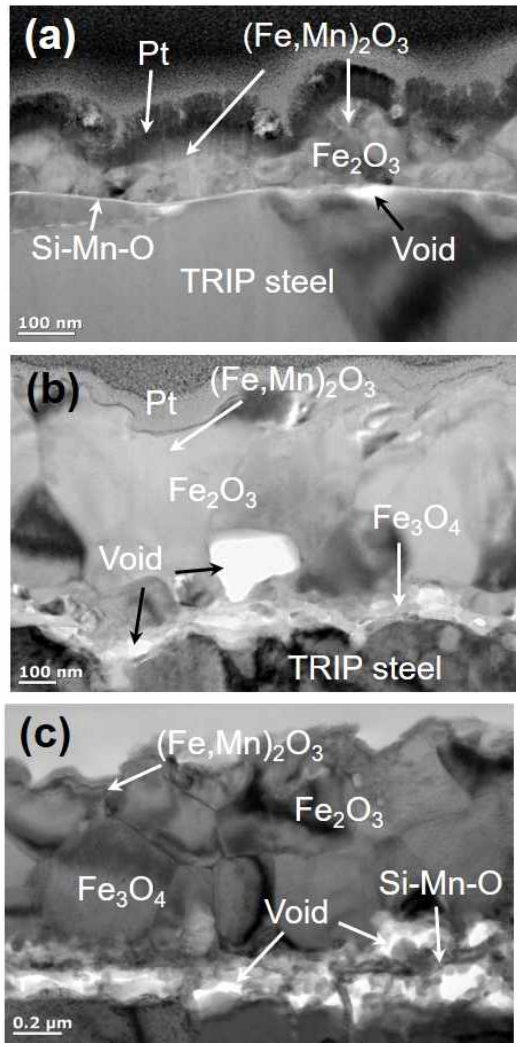

Fig. 7 Cross-sectional TEM micrographs showing the scales formed after extended oxidation at 700 °C for 60 s under different ambient conditions: (a) N_2 + 1% O_2, (b) N_2 + 21% O_2, and (c) 100% O_2. Note that the micrographs were taken at different magnifications.

TEM in conjunction with EDX, and is presented in Fig. 7. The scale thicknesses measured from the cross-sectional TEM micrographs are listed in Table 2, where they are compared with the thicknesses without the extended oxidation at 700 °C. As shown in Fig. 7a for the case of 1% O_2, no significant scale growth occurred during the extended oxidation. There was a thin amorphous oxide layer, which was rich in Si, underneath the Fe oxide scale. The EDX analysis revealed that the top region of the scale contained a significant amount of Mn, as much as 20 at%, in accordance with the GDOES result. Since no MnO peaks were detected from the GIXRD analyses, the Mn enriched on the top of the scale is likely to be in the

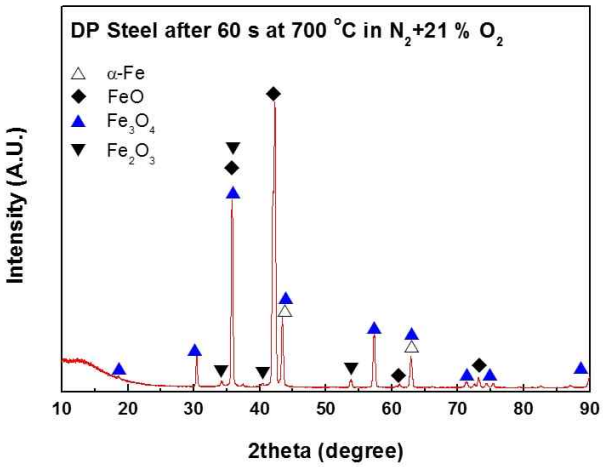

Fig. 8 GIXRD patterns for a dual phase steel sheet oxidized at 700 °C for 60 s under N_2 + 21% O_2 ambience by following the same thermal cycle as the TRIP steel samples. The dual phase steel was low in Si, with a composition of 0.02 wt% Si and 0.25 wt% Mn.

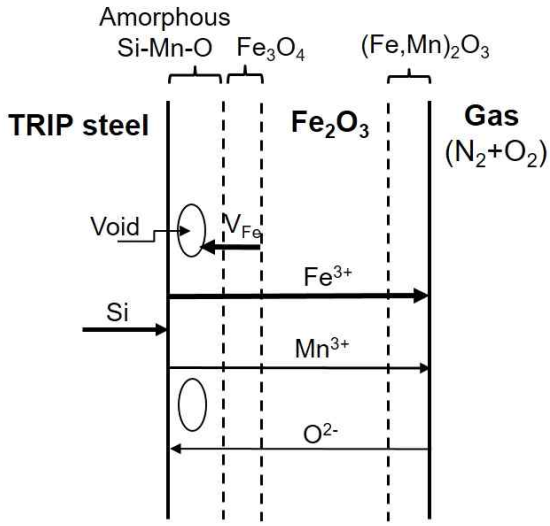

Fig. 9 Schematic illustration of the elemental transports involved in the scale growth and void formation in the present study.

form of $(Fe,Mn)_2O_3$. As can be seen in Fig. 7b and c, the scale significantly grew when extended oxidation was performed in 21% and 100% O_2 atmospheres. In accordance with the GDOES results, the Mn content on top of the scale decreases with increasing P_{O_2}, as listed in Table 3. Moreover, a greater number of voids formed in the amorphous layer of a Si-rich oxide underneath the scale with increasing P_{O_2}.

Table 3 EDX results from the top surface regions of the scales shown in Fig. 7

O_2 content (vol.%)	Composition (at.%)		
	Fe	Mn	O
1	23.90	20.33	55.77
21	30.13	8.90	60.98
100	34.74	4.41	60.84

4. Discussion

Regardless of P_{O_2} (0.01, 0.21, and 1 atm) in the oxidizing atmosphere, the TRIP steel exhibited scales with a multi-layered structure of $(Fe,Mn)_2O_3/Fe_2O_3/Fe_3O_4$/Si-Mn-O/steel upon heating to 700 °C or after isothermally holding at 700 °C for 60 s. The Fe_3O_4 layer was very thin in all the cases except when oxidized at 700 °C for 60 s in a 100% O_2 atmosphere. As the Fe-oxide scale grew faster with increasing P_{O_2}, there was a higher amount of void formation in the amorphous Si-rich Si-Mn-O oxide layer. These results indicate that the scale growth occurred predominantly by the outward diffusion of Fe, and the voids formed in the amorphous Si-rich oxide layer were the Kirkendall voids, formed because of the asymmetric diffusion of Fe and O across the scale layer.

It is well known that a multilayered scale composed of Fe_2O_3/Fe_3O_4/FeO/Fe is formed when a sheet of pure Fe was oxidized at temperatures above 570 °C under a P_{O_2} high enough for Fe_2O_3 to be formed at the outermost surface. Moreover, the fastest and slowest growing phases are known to be FeO and Fe_2O_3, respectively [15]. In the present study, however, the fastest growing oxide phase was Fe_2O_3, and the FeO phase was absent in the scale. This suggests that the scale growth on the TRIP steel surface should be influenced by the formation of the amorphous Si-rich oxide layer underneath the Fe oxide scale. It has been reported that the transport rate of Fe ions though an amorphous Si oxide depends on the charge state of the Fe ions, i.e., Fe^{3+} diffusing much faster than Fe^{2+} [20,21]. Accordingly, the faster transport of Fe^{3+} across the amorphous layer resulted in the preferential growth of Fe_2O_3 composed of Fe^{3+} and O^{2-}, while the formation of FeO, composed of Fe^{2+} and O^{2-}, was suppressed.

To further confirm the influence of the amorphous Si-rich oxide layer on the scale growth, a dual phase steel sheet containing 0.25 wt% Mn and 0.02 wt% Si, from which the formation of an amorphous Si-oxide layer could be neglected, was oxidized under N_2 + 21% O_2 atmosphere by following the same thermal cycle (heating and holding at 700 °C for 60 s) as the TRIP steel and then GIXRD analysis was performed for the oxide phases in the scale. As shown in Fig. 8, the GIXRD pattern ex-

hibited strong peaks of FeO and Fe_3O_4 together with minor peaks of Fe_2O_3.

The elemental transport for the scale growth and void formation in this study are schematically depicted in Fig. 9. Void formation in the amorphous Si-rich oxide layer is likely due to the presence of an Fe_3O_4 layer in between the Fe_2O_3 and amorphous layers. It is known that Fe^{3+} and cationic impurities in Fe_2O_3 diffuse by an interstitial-type or interstitialcy mechanism [22]. Therefore, the outward diffusion of Fe and Mn through the Fe_2O_3 layer would not involve an inward flow of vacancies. However, Fe ions (Fe^{2+} and Fe^{3+}) are known to diffuse by a vacancy mechanism in Fe_3O_4 [15,23]. Therefore, Fe vacancies (V_{Fe}) are likely formed at the Fe_3O_4/Fe_2O_3 interface and diffuse inward into the amorphous Si-rich layer, where they agglomerate to form voids.

In general, oxidation of a metal leading to scale growth follows linear kinetics of scale growth in the initial stage of oxidation. After a certain period of linear growth, the oxidation follows a parabolic kinetics controlled by elemental diffusion. According to the Wagner's theory, the parabolic rate constant of an n-type oxide is independent of P_{O_2} in the ambient gas when the n-type oxide grows by diffusion of cationic components [24]. However, as summarized in Table 2, the oxide scale growth in this study was greatly enhanced by increasing P_{O_2} although the dominantly growing oxide was the n-type Fe_2O_3. This implies that the rate-limiting step in the oxidation of the TRIP steel for 60 s at 700 °C was the reaction at the scale/gas interface and that the outward diffusion rate of Fe through the scale was sufficiently fast. The increased reaction rate to form Fe_2O_3 at the gas interface with increasing P_{O_2} was responsible not only for the enhanced scale growth but also for the relatively lower segregation of Mn at the scale surface and the increased void formation in the amorphous Si-Mn-O layer.

In the oxidation-reduction process for hot-dip galvanizing of TRIP steels, the amorphous Si-Mn-O layer underneath the Fe oxide scale cannot be reduced in the subsequent intercritical annealing stage and remains after hot-dip galvanizing. Therefore, the presence of voids in the amorphous Si-Mn-O layer would greatly increase the susceptibility of the Zn coating overlay being detached from the steel substrate. The present results suggest that the peroxidation should be performed under a low P_{O_2} atmosphere to suppress the void formation underneath the Fe oxide scale.

5. Summary

Oxidation behavior of a TRIP steel containing 1.6 wt% Mn and 1.5 wt% Si during the pre-oxidation stage in the oxidation-reduction scheme was examined to determine the effect of P_{O_2} in the oxidizing atmosphere. Oxidation was performed by ramping up to 700 °C at a rate of 6 °C/s and then isothermal holding at 700 °C for 60 s under three different ambient gases at 1 atm: N_2 + 1% O_2, N_2 + 21% O_2, and 100% O_2. Regardless of P_{O_2}, a multilayered scale composed of $(Fe,Mn)_2O_3/Fe_2O_3/Fe_3O_4$/Si-Mn-O/steel was formed upon heating to 700 °C. The multilayered scale structure was still maintained without the formation of FeO even after the extended oxidation at 700 °C for 60 s. The scale growth occurred predominantly by the growth of the outermost Fe_2O_3 layer for all ambient conditions, and its growth rate significantly increased with increasing P_{O_2}, implying that the scale growth was reaction-controlled at the Fe_2O_3/gas interface. The enhanced growth rate of Fe oxide scale with increasing P_{O_2} resulted in the formation of more Kirkendall voids in the amorphous Si-Mn-O layer. In contrast to the alloying element Si, which was internally oxidized at the Fe-oxide scale/steel interface, the alloying element Mn had a great tendency to be externally oxidized at the scale surface forming $(Fe,Mn)_2O_3$, which increased with decreasing P_{O_2}. The predominant growth of Fe_2O_3 and the absence of FeO in the scale formed on the TRIP steel surface were attributed to the presence of the amorphous Si-Mn-O layer through which Fe^{3+} ions diffused much faster than Fe^{2+} ions.

References

1. B. C. De Cooman, *Curr. Opin. Solid. St. M.*, **8**, 285 (2004).
2. J. Mahieu, S. Claessens, and B. C. De Cooman, *Metall. Mater. Trans. A.*, **32A**, 2905 (2001).
3. A. R. Marder, *Prog. Mater. Sci.*, **45**, 191 (2000).
4. B. Mintz, *Int. Mater. Rev.*, **46**, 169 (2001).
5. S. H. Kim, J. Y. Huh, S. K. Lee, R. B. Park, and J. S. Kim, *Corros. Sci. Tech.*, **10**, 6 (2011).
6. E. M. Bellhouse, A. I. M. Mertens, and J. R. Mcdermid, *Mat. Sci. Eng. A.*, **463**, 147 (2007).
7. Y. Suzuki, T. Yamashita, Y, Sugimoto, S. Fujita, and S. Yamaguchi, *ISIJ int.*, **49**, 564 (2009).
8. Y. F. Gong, H. S. Kim, and B. C. De Cooman, *ISIJ Int.*, **48**, 1745 (2008).
9. Y. F. Gong, H. S. Kim, and B. C. De Cooman, *ISIJ Int.*, **49**, 557 (2009).
10. T. Van De Putte, D. Loison, J. Penning, and S. Claessens, *Metall. Mater. Trans. A.*, **39**, 2875 (2008).
11. X. S. Li, S. I. Baek, C. S. Oh, S. J. Kim, and Y. W. Kim, *Scripta. Mater.*, **57**, 113 (2007).
12. L. Cho, S. J. Lee, M. S. Kim, Y. H. Kim, and B. C. De Cooman, *Metall. Mater. Trans. A*, **44**, 362 (2013).
13. M. Norden, M. Blumenau, T. Wuttke, and K. Peters, *Appl. Surf. Sci.*, **271**, 19 (2013).

14. L. Bordignon, X. Vanden Eynde, and R. Fransen, *Rev. Métall.*, **101**, 559 (2004).
15. W. Schwenk and A. Rahmel, *Oxid. Met.*, **25**, 293 (1986).
16. I. Parezanovic and M. Spiegel, *Surf. Eng.*, **20**, 285 (2004).
17. T. Adachi and G. H. Meier, *Oxid. Met.*, **27**, 347 (1987).
18. M. Fukumoto, S. Maeda, S. Hayashi, and T. Narita, *Oxid. Met.*, **55**, 401 (2001).
19. P. R. S. Jackson and G. R, Wallwork, *Oxid. Met.*, **20**, 1 (1983).
20. A. Atkinson and J. W. Gardner, *Corros. Sci.*, **21**, 49 (1981).
21. S. Bhagwat, S. N. Yedave, D. M. Phase, S. M. Chaudhari, S. M. Kanetkar, and S. B. Ogale, *Phys. Rev. B*, **40**, 700 (1989).
22. K. Hoshino and N. L. Peterson, *J. Phys. Chem. Solids.*, **46**, 1247 (1985).
23. S. Hallstrom, L. Hoglund, and J. Agren, *Acta. Mater.*, **59**, 53 (2011).
24. N. Birks, G. H. Meier, and F. S. Pettit, *Introduction to high temperature oxidation of metals, 2nd ed.*, Cambridge University Press, Cambridge (2006).